MERIS Atmospheric Water Vapor Correction Model for Wide Swath Interferometric Synthetic Aperture Radar

Zhenhong Li, *Member, IEEE*, Paolo Pasquali, Alessio Cantone, Andrew Singleton, Gareth Funning, and David Forrest

***Abstract*—A major source of error for repeat-pass interferometric synthetic aperture radar is the phase delay in radio signal propagation through the atmosphere, particularly the part due to tropospheric water vapor. These effects become more significant for ScanSAR observations due to their wider coverage (e.g., 400 km × 400 km for ENVISAT Advanced Synthetic Aperture Radar (ASAR) wide swath (WS) mode versus 100 km × 100 km for ASAR image mode). In this letter, we demonstrate for the first time that a Medium Resolution Imaging Spectrometer water vapor correction model can significantly reduce atmospheric water vapor effects on ASAR WS interferograms, with the phase variation in non-deforming areas decreasing from 3.8 cm before correction to 0.4 cm after correction.**

***Index Terms*—Medium Resolution Imaging Spectrometer (MERIS), radar interferometry, ScanSAR, synthetic aperture radar (SAR), water vapor correction, wide swath (WS) interferometric SAR (InSAR).**

I. Introduction

MOST synthetic aperture radar (SAR) satellites operate in stripmap (image) mode, whereby a single fixed antenna illuminates a fixed-width area, or "swath," on the ground. Since imaging resolution in the radar azimuth (along-track) direction is related to the interval between radar pulses at the same radar incidence angle, fixing the antenna allows short repeat times such that typical azimuth resolutions are meters to tens of meters [e.g., about 4 m for ENVISAT Advanced Synthetic Aperture Radar (ASAR)]. The ASAR instrument is able to switch its radar beam between seven different incidence angles in image mode (IM), its swath width varying from 56 km (swath 7, average incidence angle of 44° from the vertical) to 100 km (swath 1, average incidence angle of 19° from the vertical). Thus, although conventional IM data can image the ground at high resolution, the swath width is typically narrow.

Manuscript received July 12, 2011; revised August 11, 2011; accepted August 17, 2011. Date of publication October 6, 2011; date of current version February 8, 2012. This work was supported in part by the Natural Environmental Research Council through the GAS project (Reference: NE/H001085/1), by the National Centre of Earth Observation of which the Centre for the Observation and Modelling of Earthquakes, Volcanoes, and Tectonics is a part, by the National Natural Science Foundation of China under Grant 41074005, and by the China 863 Program under Grant 2009AA12Z317.

Z. Li, A. Singleton, and D. Forrest are with the School of Geographical and Earth Sciences, University of Glasgow, G12 8QQ Glasgow, U.K. (e-mail: Zhenhong.Li@glasgow.ac.uk).

P. Pasquali and A. Cantone are with sarmap S.A., 6989 Purasca, Switzerland.

G. Funning is with the Department of Earth Sciences, University of California–Riverside, Riverside CA 92521 USA.

Digital Object Identifier 10.1109/LGRS.2011.2166053

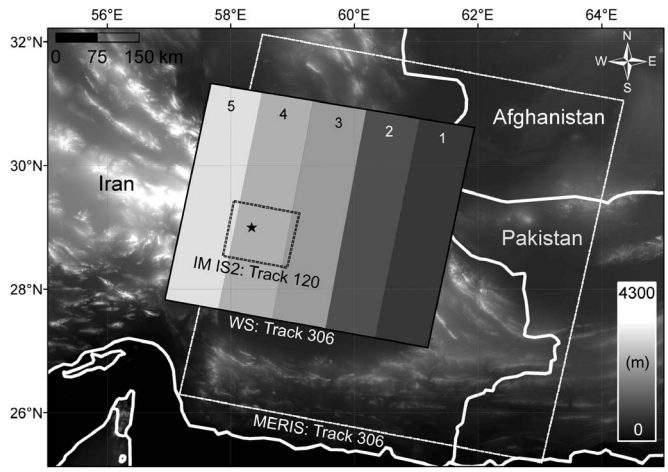

Fig. 1. Coverage of ASAR IM (small black dashed rectangle), ASAR WS (black gradational rectangle), and FR MERIS (large white dashed rectangle) over the Bam (Iran) region. (a) Black star indicates the epicenter of the 2003 Bam (Iran) earthquake [13]. (b) Black dashed rectangle denotes the coverage of ASAR image swath 2 (IS2). (c) Five stripes with different colors (from dark gray to light gray to white) in the WS track imply five subswaths.

This constraint can be overcome by utilizing the ScanSAR principle, whereby short bursts of data are acquired at different radar incidence angles. By changing the incidence angle at regular short intervals, multiple swath images (five subswaths in total for ASAR) can be obtained in a single satellite pass. These can then be combined into a single large swath, greatly increasing the areal coverage, albeit at the expense of azimuth resolution. The wide swath (WS) ASAR image generated in this way covers a region of 400 km × 400 km with a spatial resolution of c. 150 m × 150 m. The wide coverage of ScanSAR products reduces the need for postprocessing to mosaic large deformation maps and digital elevation models (DEMs) [1].

Atmospheric water vapor effects represent one of the major limitations of repeat-pass interferometric SAR (InSAR), particularly for small-amplitude geophysical signals with long wavelengths, such as interseismic deformation and some anthropogenic processes. Zebker *et al.* [2] suggested that a 20% spatial or temporal change in relative humidity could result in a 10–14-cm error in two-pass InSAR deformation retrievals, independent of baseline parameters. The wider coverage of the WS product makes it more vulnerable to tropospheric water vapor variations than the IM product, since the decorrelation distance of water vapor can be between 500 and 1000 km [3].

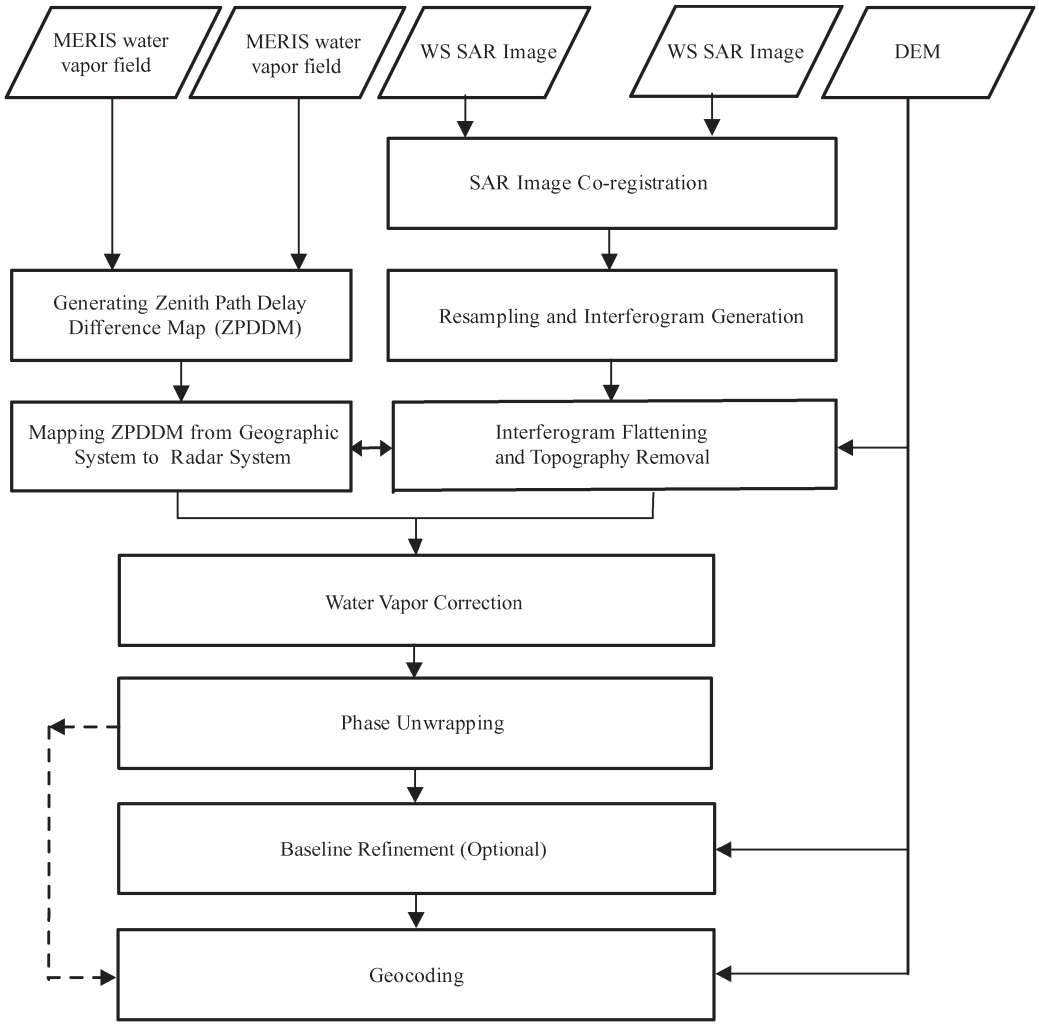

Fig. 2. Flowchart of WS InSAR processing with MERIS water vapor correction.

Space-based monitoring is an effective way to obtain global measurements of water vapor distributions with a high spatial resolution (e.g., 0.3 km $\times$ 0.3 km), and calibration techniques to spatially reduce path delays using the European Space Agency (ESA) Medium Resolution Imaging Spectrometer (MERIS) data have been successfully demonstrated [4]–[8]. Launched together with ASAR on the ESA ENVISAT spacecraft on March 1, 2002, MERIS is a passive push-broom imaging instrument and measures the solar radiation reflected from the Earth's surface and clouds in the visible and near-IR spectral ranges during the daytime [9]. MERIS has 2 out of 15 narrow spectral channels in the near IR for the remote sensing of water vapor either above land or ocean surfaces under cloud-free conditions [10] or above the highest cloud level under cloudy conditions [11]. Spatiotemporal comparisons show c. 1.1-mm agreement between MERIS and GPS/radiosonde water vapor products in terms of standard deviations [5]. MERIS near-IR data have been used to reduce water vapor effects on ASAR IM interferograms, and application of the MERIS correction models to ASAR data over the Los Angeles region showed that the order of water vapor effects on interferograms can be reduced from $\sim$10 to $\sim$5 mm after correction [6].

In this letter, we evaluate a MERIS water vapor correction model for WS InSAR. It is clear that the MERIS correction model for WS InSAR has several advantages over that for IM InSAR: 1) MERIS near-IR water vapor products are available at two nominal spatial resolutions, i.e., 0.3 km for full resolution (FR) mode and 1.2 km for reduced resolution mode, and WS images have a more comparable spatial resolution to MERIS data than IM images (150 m for WS versus 30 m for IM), and 2) the spatial coverage of WS images is also more comparable to MERIS images than that of IM images. It should be noted that WS ASAR subswath 5 does not fall within the MERIS coverage, as shown in Fig. 1.

II. MERIS Water Vapor Correction Model for WS InSAR

A MERIS water vapor correction model has been successfully incorporated into the sarmap SARscape package [12]. As shown in Fig. 2, this model involves the usual steps of image coregistration, interferogram formation, and interferogram flattening and removal of the topographic signal by use of a DEM. At this point, the integration approach diverges from the

usual interferometric processing sequence with the insertion of a zenith-path-delay difference map (ZPDDM) [6], which aims to reduce water vapor variations in interferograms before phase unwrapping. The ZPDDM is derived from cloud-free MERIS near-IR water vapor observations [4], [6], mapped from the geographic coordinate system to the radar coordinate system (range and azimuth) and subtracted from the interferogram. This corrected interferogram can be unwrapped, and an adjusted baseline can be estimated by minimizing the difference between the slant-range-projected reference DEM and a simulated height map converted from the unwrapped phase over ground control points (GCPs). Note that the baseline refinement step is optional and only desirable if there is an overall tilt in the unwrapped phase across the interferogram. The geocoding procedure maps the corrected unwrapped phase values from the radar coordinate system into the DEM-based coordinate system and converts the unwrapped phase values to range changes in the radar line of sight (LOS).

III. Application of the MERIS Model to the Bam Earthquake

A pair of ENVISAT ASAR WS images over the Bam (Iran) region on the descending (satellite moving south) track 306 (indicated as a black rectangle in Fig. 1) was processed from the ASAR level 0 (raw data) products using the SARscape software [12]. Effects of topography were removed from the interferograms using a 3-arc-second ($\sim$90 m) posting DEM produced by the Space Shuttle Radar Topography Mission (SRTM) [13]. The WS interferogram has a perpendicular baseline of 110 m, and the error in the SRTM DEM (i.e., nominally 8 m in Eurasia [13]) might lead to a phase error of up to 0.67 rad (equivalent to a range change of 0.3 cm in the radar LOS). Therefore, the topographic phase contribution can be considered negligible.

Fig. 3(a) shows the original wrapped interferogram in the radar coordinate system. Asymmetric deformation signals can be observed in the epicenter region (indicated by a black rectangle), the pattern of which is similar to the descending IM interferogram (track 120), as shown in [14, Fig. 4(b)]. It is also clear in Fig. 3(a) that there are five irregular fringes in the far field across the 400 km $\times$ 400 km region. After refining the baseline using 44 GCPs [indicated as white crosses in Fig. 3(a)], three to four irregular fringes remain in the far field [mainly in the north part of the interferogram; Fig. 3(b)]. These residual phases are caused by the spatiotemporal variations of tropospheric water vapor distribution between the acquisitions, which are evident in the ZPDDM derived from MERIS near-IR water vapor products (Fig. 4). After applying MERIS water vapor correction, five parallel fringes (oriented approximately parallel to the track direction) can be observed in the far field [Fig. 3(c)]. Note that the gray strip in the right of the corrected interferogram is due to subswath 5 being outside the MERIS coverage, as previously mentioned. As shown in Fig. 3(d), the five parallel fringes disappeared after applying baseline refinement with 33 GCPs [indicated as white crosses in Fig. 3(c)]. Phase variation of the unwrapped WS interferogram in the far field (i.e., the area that did not undergo deformation in the earthquake) decreased from 8.4 rad (equivalent to a LOS range change of 3.8 cm) without correction to 0.9 rad (equivalent to a LOS range change of 0.4 cm) after applying the MERIS water vapor correction model, implying that the unwrapped phase was much flatter after correction. Note that the reduction of the phase variation in the nondeforming area can be representative of the performance of the MERIS water vapor correction model to the WS interferogram.

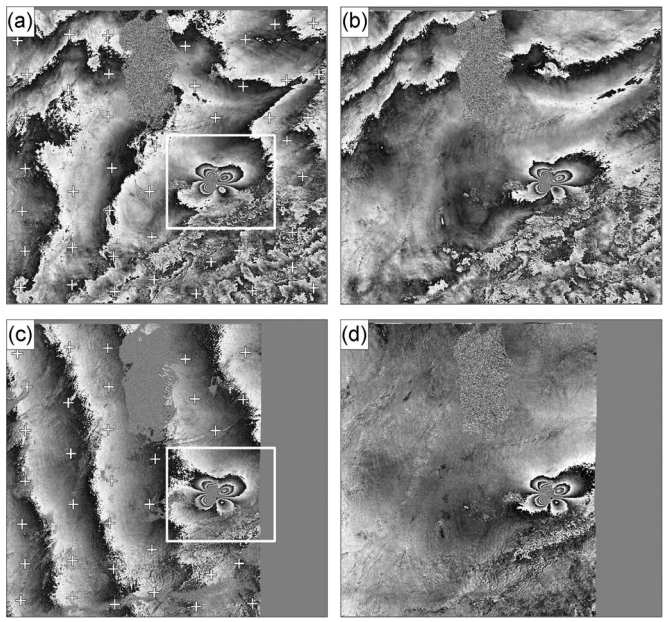

Fig. 3. WS interferogram 030902-040608 in the radar coordinate system. (a) Original interferogram before baseline refinement. (b) Original interferogram after baseline refinement. (c) Interferogram with water vapor correction. (d) Water vapor corrected interferogram after baseline refinement. Note the following: 1) white crosses in (a) and (c) represent GCPs used in baseline refinement, and 2) white rectangles in (a) and (c) denote the deforming area due to the 2003 Bam earthquake.

In order to further validate the performance of our MERIS correction model, a comparison was performed between the corrected WS interferogram and the two-fault variable-slip dislocation model of the 2003 Bam earthquake by Funning *et al.* [14]. Using IM interferograms from both ascending and descending tracks, Funning *et al.* [14] claimed that the deformation pattern observed by InSAR can be best explained by slip on two subparallel faults: one blind strike-slip fault extending under the center of Bam and a second dipping 64° W, striking parallel to, and east of, the main strike-slip fault. They showed that the root-mean-square (rms) misfit of observed-to-modeled ground displacements was 1.3 cm in the near field with some residual fringes remaining due to unmodeled fault complexity.

The water vapor corrected WS interferogram is shown in Fig. 5(a), the model WS interferogram in Fig. 5(b), and their residuals in Fig. 5(c). It is clear that the two-fault variable-slip model by Funning *et al.* [14] can reproduce the main features of the WS interferogram. The misfit to the WS data in the near field is 1.1 cm, which is on the same order of that to the IM data (i.e., 1.3 cm) [14]. Note that the difference in the rms misfit values obtained can be attributed to the different source of interferograms and the sampling of the interferograms. On close inspection of the residual WS interferogram, it is found that the pattern of the remaining residual fringes

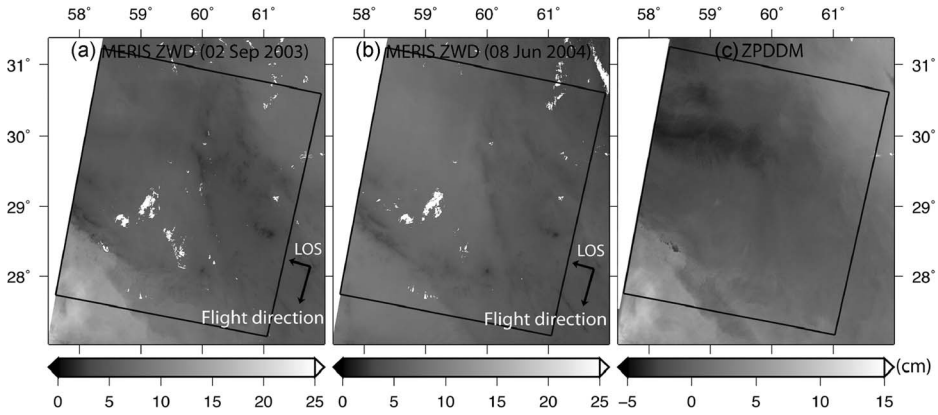

Fig. 4. (a) Zenith wet delays (ZWDs) derived from MERIS near-IR water vapor products on September 2, 2003. (b) ZWD derived from MERIS near-IR water vapor products on June 8, 2004. (c) $ZPDDM = ZWD^b - ZWD^a$. Note the following: 1) a conversion factor of 6.2 was employed to convert water vapor to ZWD, which can be calculated using surface temperature measurements obtained from radiosondes [3], and 2) black rectangles denote the coverage of Fig. 3(c) and (d) and are identical to the coverage of the geocoded WS interferogram after water vapor correction, as shown in Fig. 5(a).

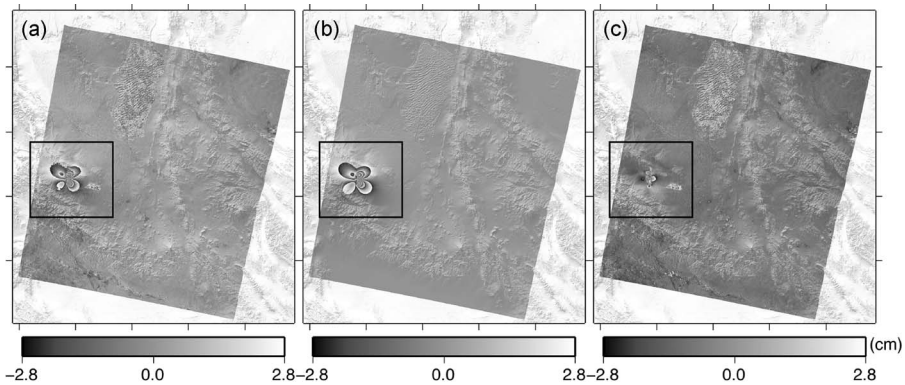

Fig. 5. WS interferograms superimposed on an SRTM DEM. (a) Corrected WS interferogram using MERIS correction model. (b) Modeled WS interferogram from the two-fault variable-slip model of the Bam earthquake by Funning *et al.* [14]. (c) Residual interferogram. Note that black rectangles denote the deforming area due to the 2003 Bam earthquake.

is similar to that of the descending IM interferogram shown in [14, Fig. 12(b)]. The rms misfit of observed-to-modeled ground displacements to the whole corrected WS interferogram is 0.6 cm. It is worth pointing out that the rms misfit to the original WS interferogram (without water vapor correction) is 3.1 cm, suggesting a reduction of 2.5 cm due to tropospheric water vapor effects in the WS interferogram in reference to the variable-slip dislocation model by Funning *et al.* [14].

IV. Discussion and Conclusion

This letter has demonstrated a MERIS water vapor correction model for WS InSAR for the first time. This correction model has been successfully incorporated into the commercial SARscape package, and its application to ASAR WS data suggests that the uncertainty in WS interferograms can be decreased from 3.8 cm before correction to 0.4 cm after correction.

There are two limitations of the MERIS water vapor correction model: 1) the MERIS correction model is only applicable under cloud-free conditions, since MERIS near-IR water vapor products are sensitive to the presence of clouds, and it should be noted that the Middle East, North Africa, South Africa, Australia, Chile, Antarctica, Southern California, and North Mexico still show cloud-free frequencies as high as 60% or even more [4], and 2) the MERIS correction model only works for ASAR subswaths 1, 2, 3, and 4, as subswath 5 does not fall within the MERIS coverage (Fig. 1).

An online system called Online Services for Correcting Atmosphere in Radar (OSCAR) is being developed at the Jet Propulsion Laboratory to provide estimates of the atmospheric path delays for SAR images and InSAR pairs. OSCAR uses a variety of different data sources to estimate tropospheric water vapor at high spatial resolutions for any chosen SAR image date and time. Current data sources include water vapor measurements from the National Aeronautics and Space Administration (NASA) Moderate Resolution Imaging Spectrometer (MODIS) and the European Centre for Medium-Range Weather Forecasts, and advanced interpolation techniques have been developed to make estimates where MODIS observations are not available [15]. Water vapor measurements from MERIS, the NASA Atmospheric Infrared Sounder, and GPS in certain areas with high-density networks will be employed to correct for the atmospheric effects of InSAR observations in the OSCAR system in the near future. Our recent validation study showed that the OSCAR-derived water vapor estimates agreed well with GPS water vapor products, with a correlation coefficient of 0.96 and a standard deviation of 2 mm [16], suggesting that OSCAR-based water vapor corrections show promise for improving WS InSAR measurements.

ACKNOWLEDGMENT

All ENVISAT synthetic aperture radar and MERIS data are copyrighted by the European Space Agency and were provided under project AO-6440. The authors would like to thank J. M. Lopez-Sanchez and an anonymous reviewer for the constructive reviews.

REFERENCES

[1] J. Holzner and R. Bamler, "Burst-mode and ScanSAR interferometry," *IEEE Trans. Geosci. Remote Sens.*, vol. 40, no. 9, pp. 1917–1934, Sep. 2002.

[2] H. A. Zebker, P. A. Rosen, and S. Hensley, "Atmospheric effects in interferometric synthetic aperture radar surface deformation and topographic maps," *J. Geophys. Res.*, vol. 102, no. B4, pp. 7547–7563, 1997.

[3] T. R. Emardson, F. H. Webb, and P. O. J. Jarlemark, "Analysis of water vapor spatial variability using GPS, InSAR, microwave radiometer, and radiosonde data," Jet Propulsion Lab., Pasadena, CA, 2002.

[4] Z. Li, E. J. Fielding, P. Cross, and R. Preusker, "Advanced InSAR atmospheric correction: MERIS/MODIS combination and stacked water vapour models," *Int. J. Remote Sens.*, vol. 30, no. 13, pp. 3343–3363, Jan. 2009.

[5] Z. Li, J.-P. Muller, P. Cross, P. Albert, J. Fischer, and R. Bennartz, "Assessment of the potential of MERIS near-infrared water vapour products to correct ASAR interferometric measurements," *Int. J. Remote Sens.*, vol. 27, no. 2, pp. 349–365, Jan. 2006.

[6] Z. Li, E. J. Fielding, P. Cross, and J.-P. Muller, "Interferometric synthetic aperture radar atmospheric correction: MEdium Resolution Imaging Spectrometer and Advanced Synthetic Aperture Radar integration," *Geophys. Res. Lett.*, vol. 33, p. L06816, Mar. 2006.

[7] B. Puysségur, R. Michel, and J. Avouac, "Tropospheric phase delay in interferometric synthetic aperture radar estimated from meteorological model and multispectral imagery," *J. Geophys. Res.*, vol. 112, p. B05419, May 2007.

[8] W. Xu, Z. Li, X. Ding, G. Feng, D. Hu, J. Long, H. Yin, and E. Yang, "Correcting atmospheric effects in ASAR interferogram with MERIS integrated water vapor data," *Chin. J. Geophys.*, vol. 53, no. 5, pp. 1073–1084, May 2010.

[9] *MERIS Product Handbook*, ESA: Paris, France, 2006, Issue 2.1.

[10] R. Bennartz and J. Fischer, "Retrieval of columnar water vapour over land from back-scattered solar radiation using the Medium Resolution Imaging Spectrometer (MERIS)," *Remote Sens. Environ.*, vol. 78, no. 3, pp. 274–283, Dec. 2001.

[11] P. Albert, R. Bennartz, and J. Fischer, "Remote sensing of atmospheric water vapor from backscattered sunlight in cloudy atmospheres," *J. Atmos. Oceanic Technol.*, vol. 18, no. 6, pp. 865–874, Jun. 2001.

[12] SARscape, Sarmap. [Online]. Available: http://www.sarmap.ch/pdf/SARscapeTechnical.pdf

[13] T. G. Farr, P. A. Rosen, E. Caro, R. Crippen, R. Duren, S. Hensley, M. Kobrick, M. Paller, E. Rodriguez, L. Roth, D. Seal, S. Shaffer, J. Shimada, J. Umland, M. Werner, M. Oskin, D. Burbank, and D. Alsdorf, "The Shuttle Radar Topography Mission," *Rev. Geophys.*, vol. 45, no. 2, p. RG2004, May 2007.

[14] G. J. Funning, B. Parsons, T. J. Wright, J. A. Jackson, and E. J. Fielding, "Surface displacements and source parameters of the 2003 Bam (Iran) earthquake from Envisat Advanced Synthetic Aperture Radar imagery," *J. Geophys. Res.*, vol. 110, p. B09406, Sep. 2005.

[15] P. von Allmen, E. Fielding, E. Fishbein, Z. Xing, L. Pan, M. Lo, and Z. Li, "OSCAR: Online services for correction of atmosphere in radar," in *Proc. ESTF*, Pasadena, CA, 2011, pp. 1–5.

[16] P. von Allmen, Z. Xing, E. Fielding, E. Fishbein, L. Pan, and Z. Li, "OSCAR: Online service for correcting atmosphere in radar," in *Proc. AGU Fall Meeting*, San Francisco, CA, 2010.